Eur Biophys J (2011) 40:891–905
DOI 10.1007/s00249-011-0707-2

ORIGINAL PAPER

Non-ideal mixing and fluid–fluid immiscibility in phosphatidic acid–phosphatidylethanolamine mixed bilayers

Patrick Garidel · Christof Johann · Alfred Blume

Received: 8 December 2010 / Revised: 8 April 2011 / Accepted: 27 April 2011 / Published online: 20 May 2011

Abstract Differential scanning calorimetry (DSC) was used to study the miscibility of phosphatidic acids (PAs) with phosphatidylethanolamines (PEs) as a function of chain length ($n = 14$, 16) and degree of ionization of PAs at pH 4, pH 7, and pH 12. Phase diagrams were constructed using temperature data for onset and end of the phase transition obtained from the direct simulation of the heat-capacity curves. The phase diagrams were analyzed by simulations of the coexistence curves utilizing a four-parameter regular solution model. For PA–PE mixtures, the non-ideality parameters are a function of composition indicating non-symmetric non-ideal mixing behavior. At pH 7, where the PA component is negatively charged, the systems DMPA:DMPE and DPPA:DPPE have positive non-ideality parameters ρ_1 in both phases, indicating a preferred aggregation of like molecules. In contrast, DMPA:DPPE and DPPA:DMPE mixtures had negative ρ_1 values. Measurements at pH 4 showed that mixed pair formation is favored when PA is protonated. At pH 12 where PA is doubly charged, highly positive ρ_{11} parameters are obtained for the liquid-crystalline phase except for the system DPPA:DPPE ($\rho_1 < 0$). This indicates clustering of like molecules and possibly domain formation in the liquid-crystalline phase. DPPA:DMPE at pH 12 even shows a miscibility gap in the liquid-crystalline phase. Obviously, despite the presence of doubly charged PA a fluid–fluid immiscibility is induced.

P. Garidel · C. Johann · A. Blume (✉)
Institute of Chemistry—Physical Chemistry, Martin-Luther-University Halle-Wittenberg, von-Danckelmann-Platz 4, 06120 Halle, Saale, Germany
e-mail: alfred.blume@chemie.uni-halle.de

Keywords Phosphatidic acid · Phosphatidylethanolamine · Lipid mixtures · Non-ideal mixing · Non-ideality parameter · Miscibility gap

Introduction

The lipid composition of biological membranes is extraordinarily complex—*we live in a world of mixtures*—and this complexity serves the purpose of providing proteins with the correct lipid micro environment for optimum physiological activity (Cronan and Gelman 1975; Benga and Holmes 1984). For example, in the erythrocyte membrane, with its wide range of functions and, therefore, complexity of membrane proteins (Steck 1974) a large number of lipid species are found. Van-Golde et al. (1967) reported that the human red blood cell contains at least twenty different molecular species of phosphatidylcholine and a total pool of approximately 150–200 chemically different lipid molecules. The complexity of lipid composition has attracted increasing interest and the term "lipidomics" has been coined to describe the diversity of lipid structures, the consequences for the biological system, and the different methods necessary to elucidate the structures and functions of the different lipid species (Cai et al. 2010; Shevchenko and Simons 2010).

However, biological systems composed of only a few different lipid species are also known. A study of the cell envelope of *Escherichia coli* membranes has shown that these membranes are mainly composed of two kinds of phospholipid (Cronan and Vagelos 1972)—10–15% (*w*/*w*) of the total lipid pool is phosphatidylglycerol (PG) and the main lipid fraction is 80% (*w*/*w*) phosphatidylethanolamine (PE) (Gally et al. 1980).

Interest in the mixing behavior of lipids in bilayer membranes has continually increased in recent years, because the notion of the existence of inhomogeneous lipid distribution in membranes, postulated and experimentally found in model systems more than 30 years ago (Schimshick and McConnell 1973; Wu and McConnell 1975; Aloia et al. 1988), has found its way into the analysis of biological membranes containing proteins. Many reviews have appeared, which in particular were focused on the nature of the so-called "lipid rafts" in mixtures containing cholesterol (Goñi et al. 2008; Feigenson 2009; Lingwood and Simons 2010; Coskun and Simons 2010). The more general problem of lipid miscibility and the different experimental and theoretical approaches used in the analysis of lipid mixtures have been reviewed recently by Almeida (2009).

This study deals with pseudobinary phospholipid mixtures composed of phosphatidic acid (PA) and phosphatidylethanolamine (PE). The terminology of pseudo-binary mixtures refers to a system composed of two lipid components in a large excess of water (third component) (Johann et al. 1996). The miscibility of lipids in these pseudo-binary mixtures is reflected in the shape of the pseudo-binary phase diagram, where the temperatures of onset and end of the gel to liquid–crystal phase transition are plotted versus the composition of the mixture. Therefore, determination and analysis of phase diagrams are useful for examining the mixing properties of the lipid components within the bilayer plane in both phases, both the gel and the liquid-crystalline phase.

The PA:PE mixtures were investigated as a function of the chain length of the components ($n = 14$, 16) and as a function of the ionization state of the acidic component. This type of lipid mixture is an example of a system in which both the PA and the PE headgroup are relatively small and have the ability to form intermolecular hydrogen bonds between neighboring headgroups. In addition, the charge of the PA headgroup can be modified by changing the pH from 4 to 12, i.e. going from the partially protonated form (charge $= -0.5$) to the doubly negatively charged form at pH 12. For the PE component a change of the pH from 7 to 12 leads to deprotonation of the NH_3^+ group so that the molecule becomes negatively charged whereas at neutral pH or at pH 4 the headgroup is zwitterionic (Blume and Eibl 1981).

Differential scanning calorimetry (DSC) was used to establish the binary phase diagrams of the following PA:PE systems at pH 4, 7, and 12 in pure water: DMPA:DMPE, DPPA:DPPE, DMPA:DPPE, and DPPA:DMPE. The temperatures describing the beginning and ending of the melting of the mixtures were determined by direct simulation of the heat-capacity curves utilizing the approximation of regular solution theory (Hildebrandt 1929; Lee 1975a, b, 1977a, b, 1978; Brumbaugh and Huang 1992) as described elsewhere (Johann et al. 1996; Garidel et al. 1997a). The model used for simulation of the *cp* curves includes a nonideality parameter for both phases (index "g" for the gel phase and "l" for the liquid-crystalline phase) which takes into account all non-idealities caused by mixing both components in the corresponding phase. The broadening of the heat-capacity curve, because of limited cooperativity of the mixtures, was also included in the model (Johann et al. 1996; Garidel et al. 1997a). On the basis of the temperature data obtained, phase diagrams were generated using a four-parameter Bragg-Williams approximation for non-ideal and non-symmetric mixing.

We will show that mixing of lipids in the gel and in the liquid-crystalline phase is affected by chain-length differences but also by the property of the lipid headgroup, namely its ionization state and its concomitant capability for intermolecular hydrogen bonding between headgroups. In the presence of a chain length difference between PE and PA, even partial immiscibility at pH 12 in the liquid-crystalline phase can be observed, despite the fact that both lipids are negatively charged with doubly charged PA and singly charged PE.

Materials and methods

1,2-Dimyristoyl-*sn*-glycero-3-phosphatidic acid (DMPA), 1,2-dipalmitoyl-*sn*-glycero-3-phosphatidic acid (DPPA), 1,2-dimyristoyl-*sn*-glycero-3-phosphoethanolamine (DMPE), and 1,2-dipalmitoyl-*sn*-glycero-3-phosphoethanolamine (DPPE) were obtained from Sygena (Liestal, Switzerland). The purity of the lipids was checked by thin-layer chromatography (TLC), by analogy with the method described by Garidel (1993). Because the TLC plate showed only one spot, the lipids were used without further purification. Lipid mixtures in a large excess of pure water were prepared as described in detail in our previous papers (Garidel et al. 1997a, b).

In brief, DSC measurements were performed with a MicroCal (Northampton, MA, USA) MC-2 differential scanning calorimeter. We measured three individual samples for each composition with a total concentration of 2.5 mg/ml, to test the reproducibility of sample preparation, and also performed three heating–cooling cycles. The accuracy of the DSC experiments was ±0.1°C for the main phase transition temperature T_m and ±0.2 kcal/mol for the main phase transition enthalpy ΔH_m. In addition, we checked for possible hydrolysis of the samples after the DSC measurements. TLC indicated slight decomposition of the phospholipids after the DSC runs at pH 12, so here only the first scan was evaluated. For measurements at pH 7 and 4 no decomposition was observed, here the third heating scan is shown.

Theory and simulation methods

Calculation of the heat-capacity curves

The simulation routine requires, for simulation of the heat-capacity curves, thermodynamic data for the pure components and the composition of the mixture. For simulation of the heat-capacity curves we used a model in which the excess enthalpy for both phases is described by:

$$\Delta G^E = \Delta H^E = x \cdot (1 - x) \cdot \rho$$

where ρ is the non-ideality parameter. Positive ρ values lead to demixing of the two components whereas negative ρ values are characteristic of preferential pair-formation of unlike pairs. This is the so-called "regular solution" model, in which the excess entropy of mixing is zero. This model can be used when both components have similar size. The fitting parameters for the heat-capacity curves are then two non-ideality parameters, one for each phase, and the van′t Hoff transition enthalpy describing the broadening of the phase transition caused by limited cooperativity (Mennicke 1995; Johann et al. 1996; Garidel et al. 1997a). In addition, the temperatures at the onset (T_-) and end (T_+) of the phase transition, i.e., the temperatures defining the *solidus* and *liquidus* curves, are calculated for a binary mixture in which a pseudo-first-order phase transition is assumed for the two components. It turned out that simulation of the heat-capacity curves led to ρ values which depended on the composition of the mixture, necessitating the implementation of a more refined model for simulation of the complete phase diagram.

Simulation of phase diagrams

The phase diagrams were then constructed from the onset and end temperatures of the transition determined as described above and then fitted with a refined model, accounting for non-ideal and non-symmetric mixing in both phases, because the ρ values depended on composition (see above). The detailed procedure has been described elsewhere (Johann et al. 1996; Garidel et al. 1997a). The shape of the phase diagram is mainly determined by the ρ values for the gel and the liquid-crystalline phase. However, the difference between these two values is also of major importance, it describes the changes in mixing occurring during the phase transition. When $\Delta\rho$ is positive, the phase transition induces either less pair formation or even demixing in the fluid phase depending on the ρ value for the gel phase. For DMPE–DMPG (1:1), for instance, pair formation in the gel phase was stronger than in the liquid-crystalline phase because $\Delta\rho$ was ca. 430 cal/mol (Garidel and Blume 2000). For DMPA–DPPC (1:1) at pH 4, on the other hand, ρ values for both phases were positive and $\Delta\rho$ was also positive, with a value of ca. 870 cal/mol, leading to increased demixing in the liquid-crystalline phase (Garidel et al. 1997a).

Monte Carlo simulation of lateral lipid distribution

The lateral lipid distributions in the liquid-crystalline phase were obtained by Monte Carlo simulations carried out on a 80×80 two-dimensional triangular lattice with standard periodic boundary conditions using a fixed mole fraction x and non-ideality parameters determined from the simulations of the phase diagram at a given temperature. To achieve equilibrium, a nearest-neighbor exchange dynamic was used. At least 1.5×10^4 Monte Carlo steps were performed, i.e. each lipid was moved 15,000 times leading to a configuration that elucidates the mixing behavior of the respective system (Kawasaki 1972; Jan et al. 1984).

Results

Transition of pure components

At pH 7 in pure water PAs are negatively charged (charge $= -1.0$). The degree of ionization of PAs can be changed by altering the pH of the bulk phase. At pH 4 PAs are partly protonated and have a charge of ca. -0.5 elementary charges. Full deprotonation of the phosphatidic acids can be realized under highly alkaline conditions and, therefore, PAs have a twofold negative charge at pH 12. The effect of pH on the thermotropic phase behavior of PAs has been intensively studied (Träuble and Eibl 1974; Verkleij et al. 1974; Blume and Eibl 1979, 1981; Blume and Tuchtenhagen 1992). In our previous papers (Garidel et al. 1997a, b, 2000) we have already reported some of the characteristic effects of protonation on the mixing properties of mixtures composed of PA or PG with a zwitterionic lipid such as PC.

The effect of changing the pH to 4 on the thermotropic behavior of PEs is extremely weak. The temperature for the main phase transition is slightly increased (~ 1°C) and the phase transition enthalpy is also slightly reduced (Träuble and Eibl 1974; Boggs 1987; Cevc 1990) compared with the values at pH 7 (Blume 1988, 1991). The intrinsic pK for protonation of the phosphate group of PEs is very low, with a value of 1.9 (Tatulian 1992); even lower values of 0.32 have been reported in other publications (Standish and Pethica 1968). Apparent pK values for the amine group of phosphatidylethanolamines are between 9.6 and 11.2 (Blume and Eibl 1981; Akoka et al. 1986; Watts and Poile 1986). At pH 12 the amino group of PEs is definitely deprotonated, and the molecule is thus negatively charged. The electrostatic repulsion and the reduced ability to form

Table 1 Thermodynamic data for the main phase transition of the pure phospholipids in pure water

Lipid	pH 4			pH 7			pH 12		
	T_m/°C	$T_{1/2}$/°C	ΔH_c/kcal mol^{-1}	T_m/°C	$T_{1/2}$/°C	ΔH_c/kcal mol^{-1}	T_m/°C	$T_{1/2}$/°C	ΔH_c/kcal mol^{-1}
DMPA	52.9	1.2	5.89	51.3	1.4	7.18	21.5	2.1	4.02
DMPE	50.1	1.2	4.95	49.7	1.5	5.88	32.8	1.6	3.96
DPPA	65.4	1.5	6.90	64.7	1.1	7.74	42.7	1.1	5.69
DPPE	64.1	1.2	6.45	63.8	1.2	8.46	46.2	2.4	5.62

T_m, main phase transition temperature; $T_{1/2}$, half width of transition; ΔH_c, calorimetrically measured phase transition enthalpy

a hydrogen-bonding network are the reasons for the decrease of the main phase transition temperature at pH 12. The thermodynamic data for PAs and PEs in water adjusted to the respective pH are listed in Table 1.

Pseudobinary systems

In Figs. 1, 2, 3, 4, 5, and 6 the DSC thermograms obtained for the four binary systems are shown for measurements at pH 4, pH 7, and pH 12. The solid lines are the experimentally measured curves (cp^{exp}) and the dotted lines represent the simulated heat-capacity curves (cp^{sim}). All measurements were performed in the temperature range from 8 to 95°C, but for reasons of clarity only the temperature range in the vicinity of the phase transitions is shown.

The phase diagrams were constructed from the experimental DSC curves as described elsewhere (Johann et al. 1996; Garidel et al. 1997a). Briefly, the resulting temperatures T_- and T_+ (up and down triangles in Figs. 7, 8, 9, 10, 11, and 12) were obtained by simulating the *cp* curves, which are shown in Figs. 7, 8, 9, 10, 11, and 12. On the basis of upon these temperature data, the phase diagrams were then calculated using the four-parameter model mentioned above. In Figs. 7, 8, 9, 10, 11, and 12 the temperatures for the onset and end of the phase transition (represented as open and solid circles) obtained by using an empirical method are also shown (Johann et al. 1996; Garidel and Blume 1998; Garidel and Blume 2000; Garidel et al. 1997a, b). The differences between the non-ideality parameters of the liquid-crystalline and gel phases, which were obtained by simulation of the whole phase diagrams, are indicated in Figs. 7, 8, 9, 10, 11, and 12 as $\Delta\rho_1 = \rho_{l1} - \rho_{g1}$ and $\Delta\rho_2 = \rho_{l2} - \rho_{g2}$. The latter value describes the different asymmetry in the miscibility behavior between the liquid-crystalline and gel phases.

Inclusion of the broadening effect because of limited cooperativity in the determination of the temperatures for onset and end of melting leads to phase diagrams which are narrower than those determined by the usual empirical procedure (Johann et al. 1996; Garidel et al. 1997a, b; Garidel and Blume 1998). The nonideality parameters determined by our procedure are therefore lower than those calculated on the basis of the empirically determined T_-^{exp} and T_+^{exp} values.

DMPA:DMPE

pH 7. In Fig. 1 the heat-capacity curves of the system DMPA:DMPE at pH 7 are shown. The temperature difference for the main phase transition of the pure components is only 1.6°C. Therefore, a phase diagram with a very narrow coexistence range is obtained (Fig. 7). The phase

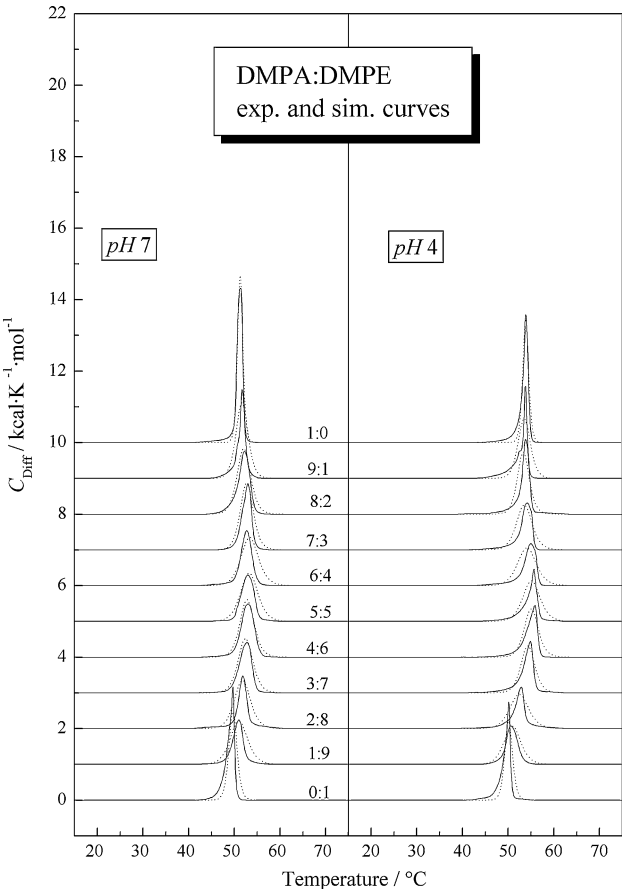

Fig. 1 DSC heating thermograms for the system DMPA:DMPE at different molar ratios at pH 7 and pH 4: experimental *cp* curves (*solid line*) and simulated *cp* curves (*dotted line*)

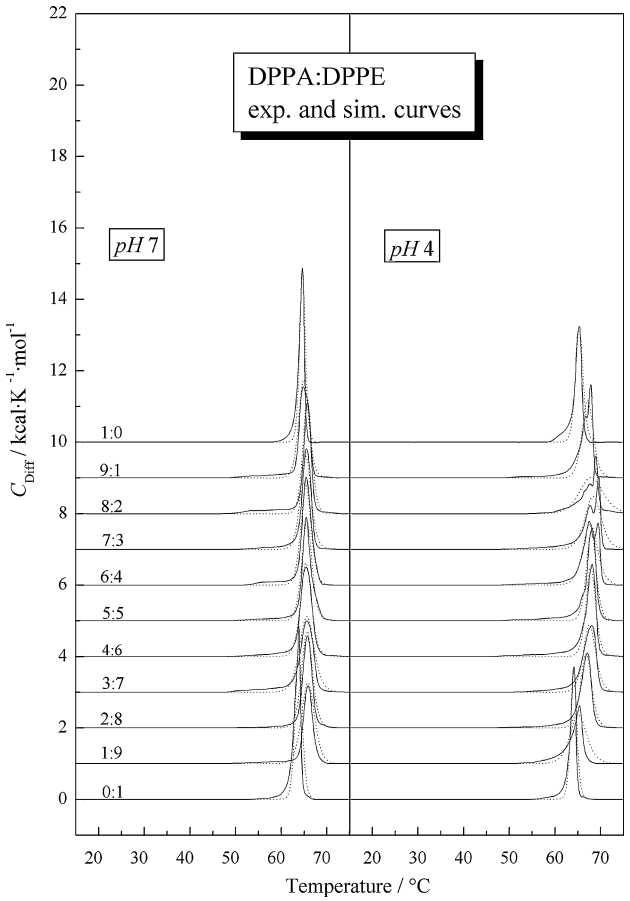

Fig. 2 DSC heating thermograms for the system DPPA:DPPE at different molar ratios at pH 7 and pH 4: experimental *cp* curves (*solid line*) and simulated *cp* curves (*dotted line*)

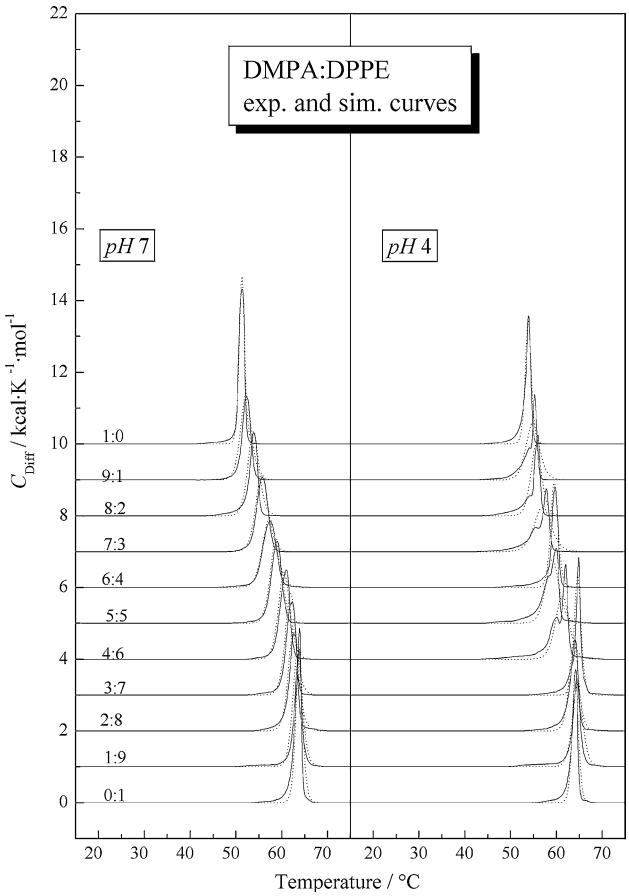

Fig. 3 DSC heating thermograms for the system DMPA:DPPE at different molar ratios at pH 7 and pH 4: experimental *cp* curves (*solid line*) and simulated *cp* curves (*dotted line*)

diagram indicates an upper azeotropic point for the equimolar mixture. The non-ideality parameters ρ_1 are both positive; a positive difference of $\Delta\rho_1 = +200$ cal/mol, as expected for a phase diagram with an upper azeotropic point, is also found (Tenchov 1985). The asymmetry parameters are both negative with $\rho_{l2} < \rho_{g2}$ with a small difference $\Delta\rho_2$. The nonideality parameters depend only weakly on the composition as can be seen from the relatively small values for ρ_{g2} and ρ_{l2} (Fig. 7).

pH 4. At pH 4 DMPA is partly protonated and the electrostatic repulsion effects on the mixing behavior should be reduced. In addition, the capability for hydrogen bonding between the headgroups is increased. The T_m value for DMPA is therefore slightly higher. The phase diagram at pH 4 (Fig. 7) has a similar shape to that at pH 7. The non-ideality parameters ρ_1 are reduced (Table 2) or even become negative for the gel phase, however the difference $\Delta\rho_1 = +148$ cal/mol remains positive. An upper azeotropic point is found again at $x_{DMPA} = 0.5$. The difference in asymmetry $\Delta\rho_2$ is negative but much more pronounced than at pH 7, which leads to higher compositional dependence of ρ.

pH 12. The thermograms of the system under alkaline conditions are shown in Fig. 5. The phase transition temperatures are shifted to lower values, which indicates destabilization of the gel phase of the systems, and the *cp* curves are broader. The simulated heat-capacity curves are in good agreement with these thermograms. The non-ideality parameters ρ obtained by simulation of the phase diagram indicate clustering of like molecules in the fluid phase, because all ρ values are positive with $\rho_l > \rho_g$ (Fig. 11). Comparison of ρ_1 with the values obtained by simulating the same system at pH 7 gives an identical value for ρ_{g1}, but the ρ value for the liquid-crystalline phase is twice as high as at pH 12 (Table 2). The difference for the asymmetry term is positive with a value of ca. +70 cal/mol. The upper azeotropic point is found at a lower amount of DMPA, namely at $x_{DMPA} = 0.35$ (Fig. 11).

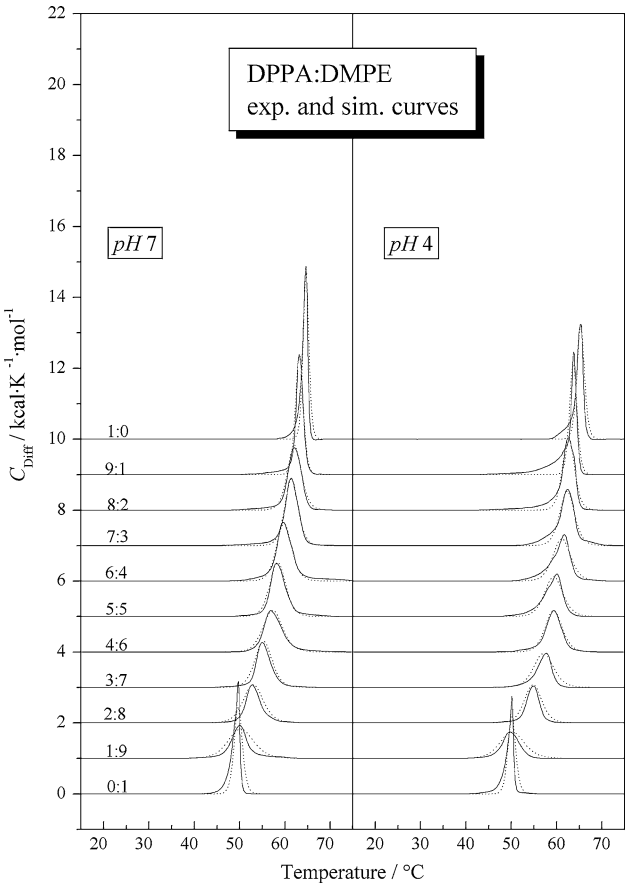

Fig. 4 DSC heating thermograms for the system DPPA:DMPE at different molar ratios at pH 7 and pH 4: experimental *cp* curves (*solid line*) and simulated *cp* curves (*dotted line*)

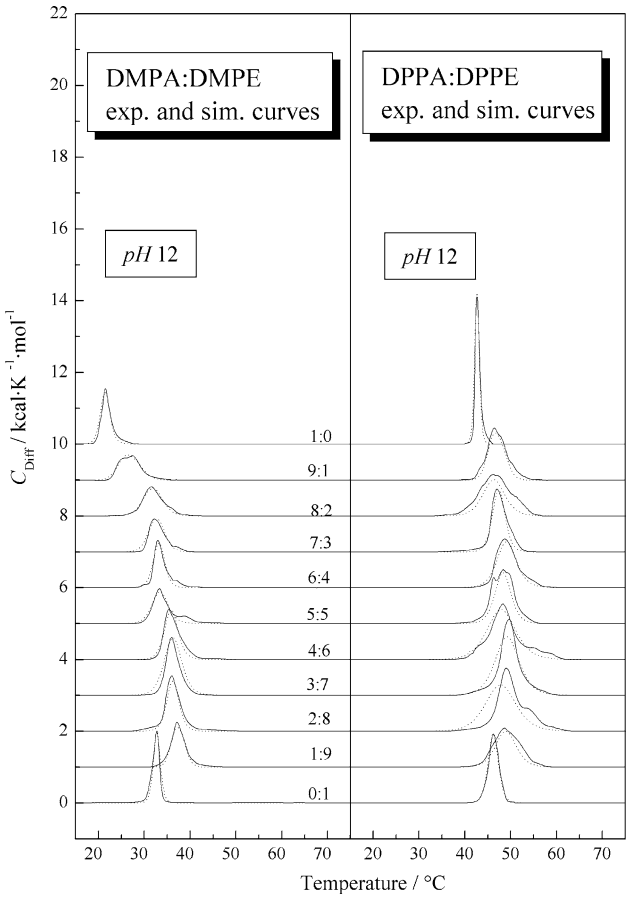

Fig. 5 DSC heating thermograms for the system DMPA:DMPE and DPPA:DPPE at different molar ratios at pH 12: experimental *cp* curves (*solid line*) and simulated *cp* curves (*dotted line*)

DPPA:DPPE

pH 7. Elongation of the chain length of both components does not have a marked effect on the miscibility properties. From the thermograms at pH 7 (Fig. 2), a phase diagram (Fig. 8) with an upper azeotropic point for an equimolar mixture of DPPA:DPPE was obtained. For the C_{16} system, all non-ideality parameters ρ are reduced compared with those for DMPA:DMPE mixtures with myristoyl chains. In addition, the difference in asymmetry, i.e. the $\Delta\rho_2$ value, is more negative, as for the system DMPA:DMPE.

pH 4. Reducing the pH to 4 has the effect that the heat-capacity curves of the mixtures for $x_{DPPA} > 0.6$ contain two peaks (Fig. 2). The upper azeotropic point is found at $x_{DPPA} = 0.6$. The nonideality parameters ρ_1 (Fig. 8) become strongly negative with $\rho_{g1} < \rho_{l1}$ leading to a positive $\Delta\rho_1$ of +279 cal/mol. The asymmetry parameters increase substantially and become positive for both phases. This trend is also found for the system DMPA:DMPE when the nonideality parameters are compared for pH 4 and pH 7. The system DPPA:DPPE is the only one having a positive $\Delta\rho_2$ at pH 4, which means that an increasing DPPA content results in an increase of $\Delta\rho$. From the obtained ρ_1 values a preference for mixed pair formation is expected.

pH 12. The thermograms of the system DPPA:DPPE system at pH 12 (Fig. 5) are broad and structured. Simulation of the phase diagram (Fig. 11) gives extremely high negative ρ_1 values with $\rho_{g1} < \rho_{l1}$ resulting in $\Delta\rho_1 = +326$ cal/mol. The asymmetry parameters are both positive giving a similar value $\Delta\rho_2$ as for the C_{14} system at pH 12.

DMPA:DPPE

pH 7. Reducing the chain length of the PA component leads to a difference in the phase transition temperature for the pure lipids of 12–13°C. Consequently, the phase diagram has a broader coexistence range (Fig. 9). The nonideality parameters obtained from simulation of the phase diagram are negative for ρ_1. $\Delta\rho_1$ has a value of +86 cal/mol. For the asymmetry parameter of the gel phase a positive value of $\rho_{g2} = +103$ cal/mol is obtained, and for

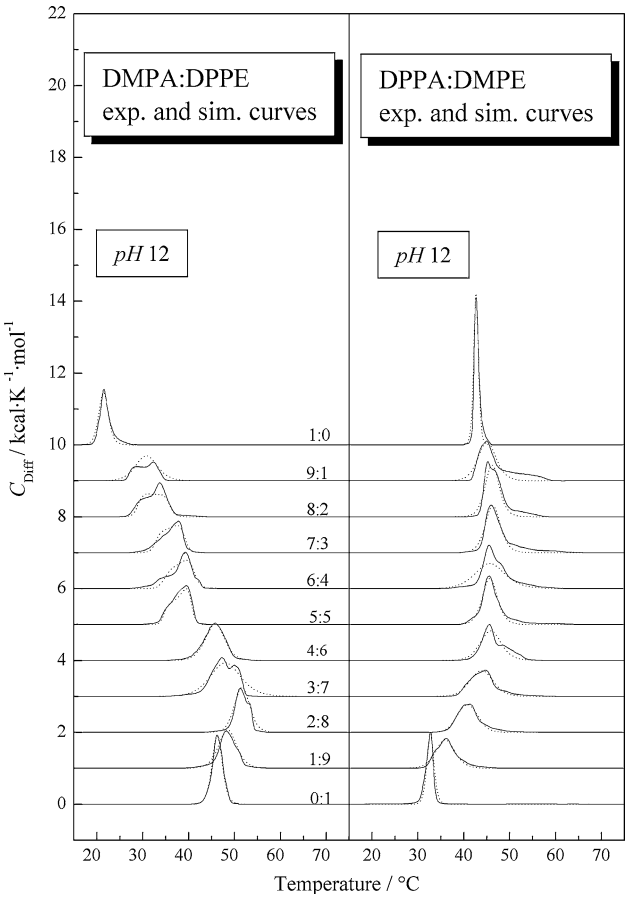

Fig. 6 DSC heating thermograms for the system DMPA:DPPE and DPPA:DMPE at different molar ratios at pH 12: experimental *cp* curves (*solid line*) and simulated *cp* curves (*dotted line*)

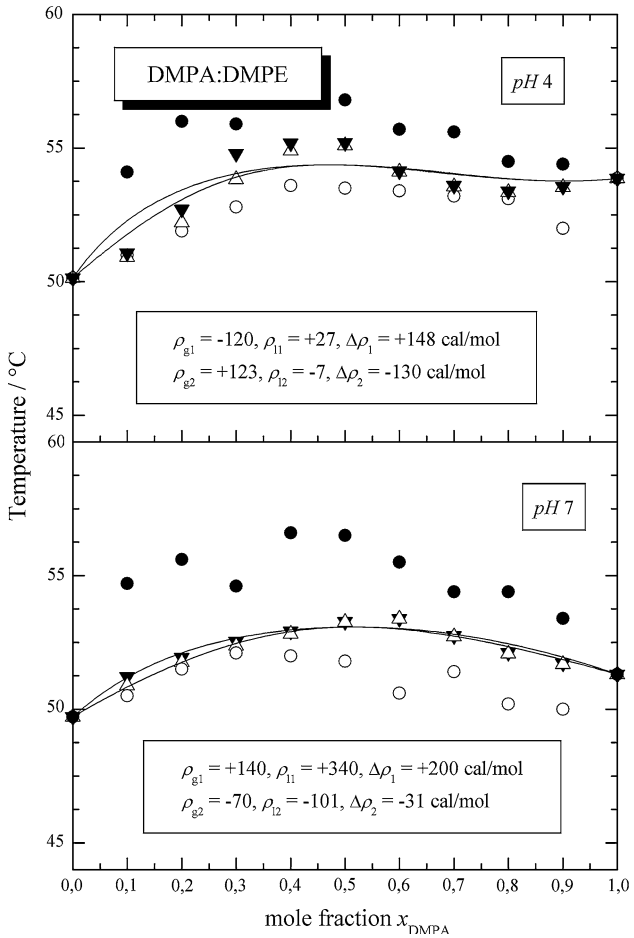

Fig. 7 Pseudo-binary phase diagrams for the system DMPA:DMPE at pH 4 and pH 7 constructed from the simulated *cp* curves. T_- and T_+ were obtained by simulation of the *cp* curves (*up* and *down triangles*). The experimentally derived T_- and T_+, represented by *circles* (*open* and *solid*), were obtained by a procedure described elsewhere (Johann et al. 1996). The *solid lines* are coexistence lines calculated using the four-parameter, non-ideal, non-symmetrical mixing model mentioned in the text. The non-ideality parameters were obtained from a nonlinear least-squares fit of the experimental data

the liquid-crystalline phase ρ_{l2} is -82 cal/mol. This results in a negative value for $\Delta\rho_2$. The difference of the non-ideality parameters $\Delta\rho$ obtained from direct simulation of the *cp* curves are in good agreement with the calculated differences of the non-ideality parameters $\Delta\rho_c$.

pH 4. Comparison of ρ values at pH 4 with those at pH 7 show the same trend as observed for the other systems. Both ρ_1 values become more negative, leading to a positive $\Delta\rho_1$ of $+90$ cal/mol, because $\rho_{g1} < \rho_{l1}$ (Fig. 9). The asymmetry parameters are both positive, yielding a negative parameter $\Delta\rho_2$ of -217 cal/mol.

pH 12. The heat-capacity curves of the system DMPA:DPPE at pH 12 (Fig. 6) show a similar trend to that observed for all other mixtures of PA:PE at this pH, namely broadening of the phase transition, and an upper azeotropic point (Fig. 12) at $x_{DMPA} = 0.2$. ρ_{g1} is negative with a value of -194 cal/mol and the corresponding parameter for the liquid-crystalline phase is $\rho_{l1} = +256$ cal/mol, which yields a positive $\Delta\rho_1$ of $+450$ cal/mol. This phase diagram shows a negative $\Delta\rho_2$ value in contrast with the other three phase diagrams at pH 12, for which $\Delta\rho_2$ is positive.

DPPA:DMPE

pH 7. In this case the chains of the PA component are longer than those of the PE component and the difference between the phase transition temperatures for the pure lipids (Fig. 4) becomes slightly larger ($\Delta T \approx 15$°C) than for the reversed case. The ρ_1 parameters are both negative and have values of ca. -290 cal/mol, leading to a vanishing $\Delta\rho_1$ parameter. The asymmetry parameter for the *liquidus* curve is slightly higher than the corresponding

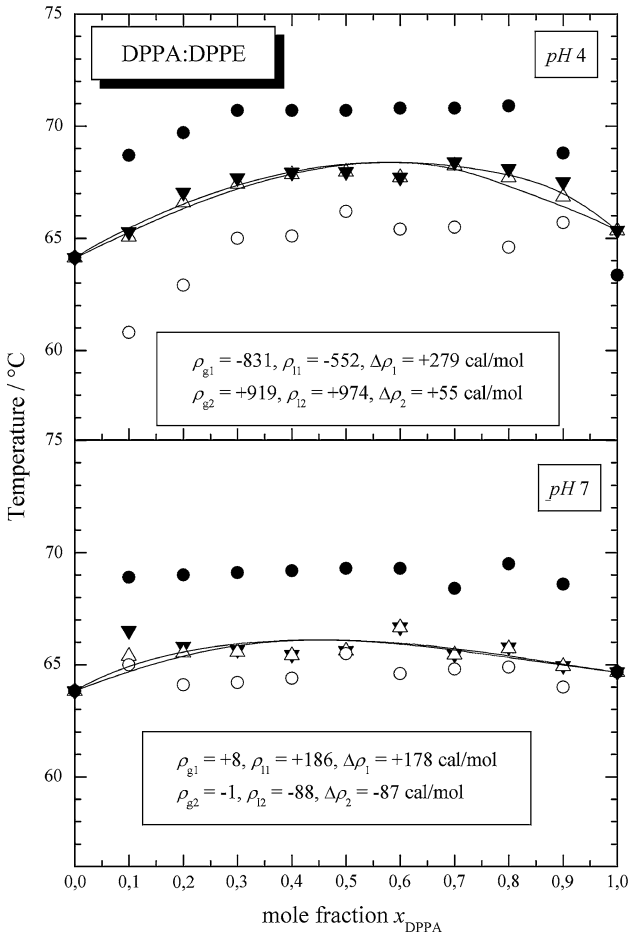

Fig. 8 Pseudo-binary phase diagrams for the system DPPA:DPPE at pH 4 and pH 7 constructed from the simulated *cp* curves. T_- and T_+ were obtained by simulation of the *cp* curves (*up* and *down triangles*). The experimentally derived T_- and T_+, represented by *circles* (*open* and *solid*), were obtained by a procedure described elsewhere (Johann et al. 1996). The *solid lines* are coexistence lines calculated using the four-parameter, non-ideal, non-symmetrical mixing model mentioned in the text. The non-ideality parameters were obtained from a nonlinear least-squares fit of the experimental data

parameter for the *solidus* curve (both ρ_2 are positive). This results in a positive difference of $\Delta\rho_2$.

pH 4. Protonation of the system DPPA:DMPE causes no significant shape changes in the phase diagram (Figs. 4 and 10) compared with the phase diagrams obtained at pH 7. Both, ρ_{g1} and ρ_{l1} are less negative for pH 4 than at pH 7, and $\rho_{g1} < \rho_{l1}$. The parameters ρ_2 are also reduced, but remain positive. The respective ρ_2 values are very similar, and therefore $\Delta\rho_2$ vanishes.

pH 12. Analysis of the heat-capacity curve of the system DPPA:DMPE at pH 12 (Fig. 6) reveals a constant end temperature of melting (T_+) for mixtures with $x_{DPPA} \geq 0.5$. On the basis of the temperature data T_- and T_+ obtained from simulation of the *cp* curves, a phase diagram was generated (Fig. 12) with a horizontal *liquidus* line in the mole fraction range $x_{DPPA} = 0.5$–0.85. If we compare this phase diagram with the diagram constructed from the empirically determined temperature data (circles in Fig. 12), this horizontal *liquidus* line could possibly be extended to x_{DPPA} ca. 0.3. The non-ideality parameters obtained from simulation of the phase diagrams are all positive. For the asymmetry term we calculate for the difference of the non-ideality parameter with $\rho_{l2} > \rho_{g2}$ a small, positive $\Delta\rho_2$ value.

Discussion

In our previous studies on the mixing behavior of pseudobinary phospholipid mixtures composed of a negatively charged lipid with a zwitterionic phospholipid

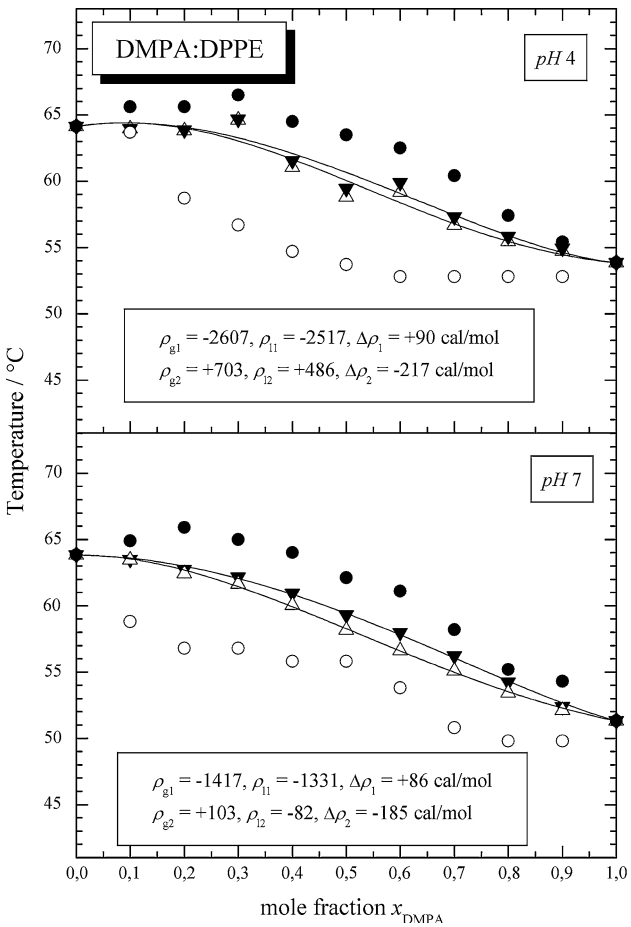

Fig. 9 Pseudo-binary phase diagrams for the system DMPA:DPPE at pH 4 and pH 7 constructed from the simulated *cp* curves. T_- and T_+ were obtained by simulation of the *cp* curves (*up* and *down triangles*). The experimentally derived T_- and T_+, represented by *circles* (*open* and *solid*), were obtained by a procedure described elsewhere (Johann et al. 1996). The *solid lines* are coexistence lines calculated using the four-parameter, non-ideal, non-symmetrical mixing model mentioned in the text. The non-ideality parameters were obtained from a nonlinear least-squares fit of the experimental data

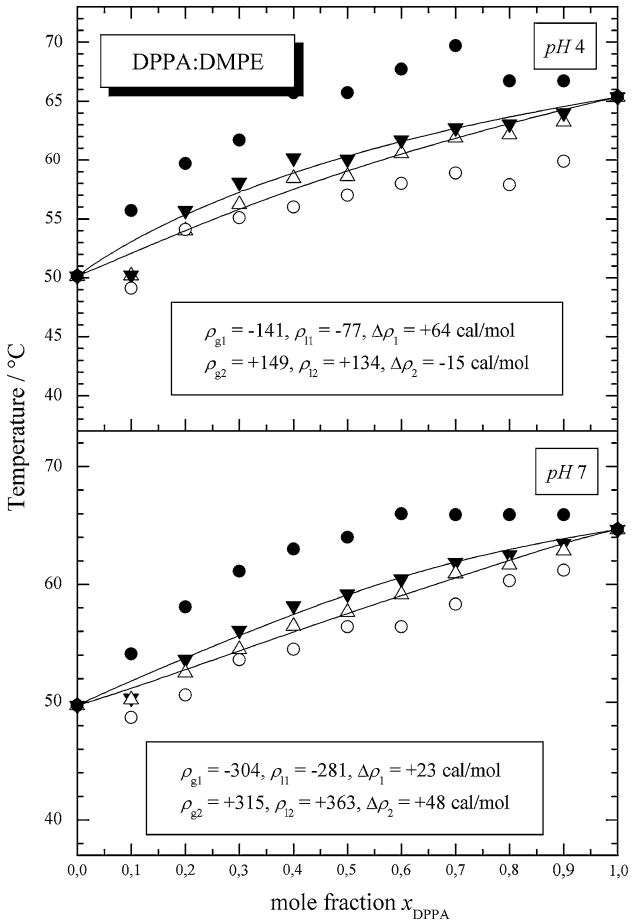

Fig. 10 Pseudo-binary phase diagrams for the system DPPA:DMPE at pH 4 and pH 7 constructed from the simulated *cp* curves. T_- and T_+ were obtained by simulation of the *cp* curves (*up* and *down triangles*). The experimentally derived T_- and T_+, represented by *circles* (*open* and *solid*), were obtained by a procedure described elsewhere (Johann et al. 1996). The *solid lines* are coexistence lines calculated using the four-parameter, non-ideal, non-symmetrical mixing model mentioned in the text. The non-ideality parameters were obtained from a nonlinear least-squares fit of the experimental data

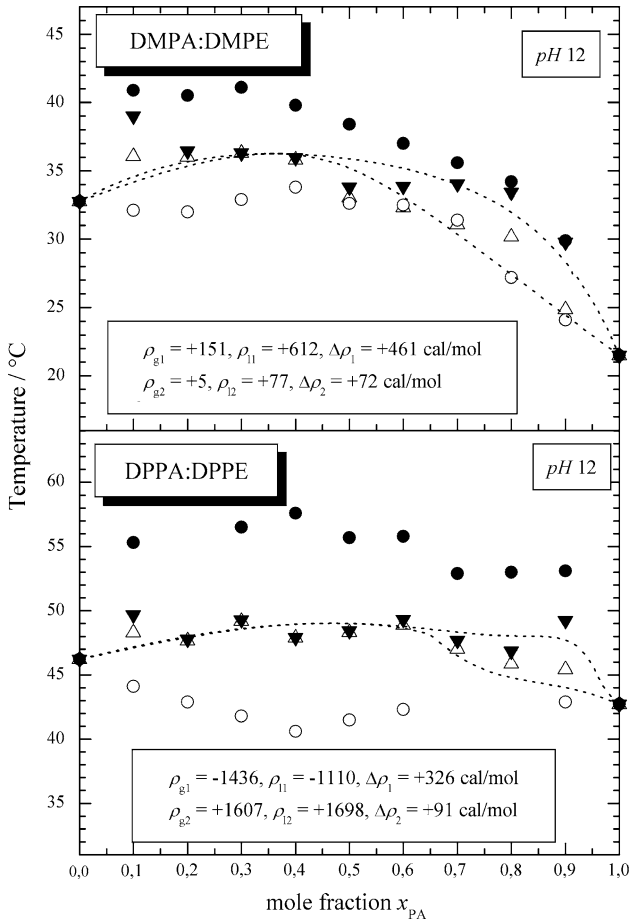

Fig. 11 Pseudo-binary phase diagrams for the systems DMPA:DMPE and DPPA:DPPE at pH 12 constructed from the simulated *cp* curves. T_- and T_+ were obtained by simulation of the *cp* curves (*up* and *down triangles*). The experimentally derived T_- and T_+, represented by *circles* (*open* and *solid*), were obtained by a procedure described elsewhere (Johann et al. 1996). The *solid lines* are coexistence lines calculated using the four-parameter, non-ideal, non-symmetrical mixing model mentioned in the text. The non-ideality parameters were obtained from a nonlinear least-squares fit of the experimental data

(Johann et al. 1996; Garidel et al. 1997a, b; 2000; 2005; Garidel and Blume 1998), we have shown the validity of the model used for direct simulation of the heat-capacity curves. Simulation of the heat-capacity curves revealed that the non-ideality parameters are a function of composition.

In this paper, the phase diagrams determined from the T_- and T_+ values (up and down triangles in Figs. 7, 8, 9, 10, 11, and 12) are refined and simulated with a thermodynamic model for non-ideal, non-symmetric mixing. This approach provides better fits than the usual two-parameter approach (see the discussion in Johann et al. 1996). The physical properties of PAs and PEs (at pH 7) are in some respects very similar. Both lipids form a strong hydrogen-bonding network (Boggs 1987) leading to similar thermodynamic data (Blume 1988). The order parameters S_{CD} obtained from ^{2}H NMR measurements also have similar values (Garidel 1993; Ziegler and Blume 1995). Both lipids form an L_β phase at pH 7. Deprotonation of PAs abolishes the possibility of intermolecular hydrogen bonding and increases the electrostatic repulsion between the lipid headgroups, which then induces a tilt of the hydrocarbon chains for PA^{2-} in the gel phase (Jähnig et al. 1979) with a concomitant decrease in transition temperature. No data are available for the effect of the degree of protonation on the tilt angle of the hydrocarbon chains of PEs. At pH 4, the phosphate group of PE is still unprotonated, so no change of acyl chain tilt is expected. At pH 12 the increased electrostatic repulsion in PE bilayers may lead to an increase in chain tilt as obtained for PAs.

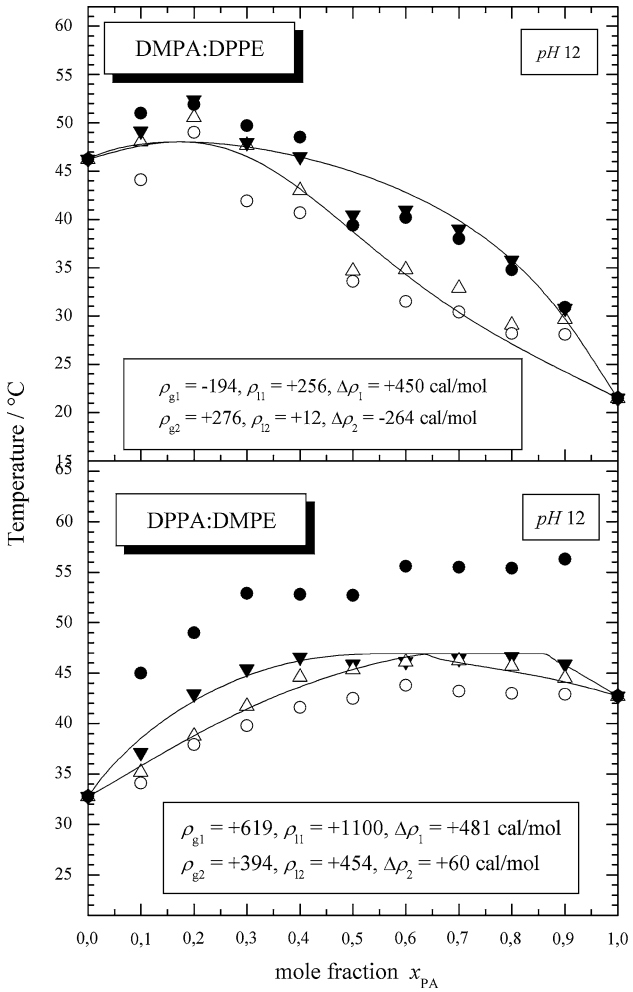

Fig. 12 Pseudo-binary phase diagrams for the systems DMPA:DPPE and DPPA:DMPE at pH 12 constructed from the simulated *cp* curves. T_- and T_+ were obtained by simulation of the *cp* curves (*up* and *down triangles*). The experimentally derived T_- and T_+, represented by *circles* (*open* and *solid*), were obtained by a procedure described elsewhere (Johann et al. 1996). The *solid lines* are coexistence lines calculated using the four-parameter, non-ideal, non-symmetrical mixing model mentioned in the text. The non-ideality parameters were obtained from a nonlinear least-squares fit of the experimental data

Pseudobinary systems at pH 7

The phase diagrams of pseudo-binary mixtures in which both components have the same chain lengths (DMPA:DMPE and DPPA:DPPE) have very similar shapes. Both phase diagrams show an upper azeotropic point at $x_{PA} = 0.5$. The non-ideality parameters ρ_1 are positive for the gel and the liquid-crystalline phase with $\rho_{l1} > \rho_{g1}$ leading to a difference of $\Delta\rho_1$ of ca. +190 cal/mol for both systems. This indicates that the tendency for clustering of like molecules is larger in the liquid-crystalline phase than in the gel phase (DMPA:DMPE). The asymmetry terms for the two mixtures are both negative with $\rho_{l2} < \rho_{g2}$ which results in a negative $\Delta\rho_2$, implying that with increasing amount of PA $\Delta\rho$ decreases.

The introduction of a chain length difference between the components of the binary system has the effect that the non-ideality parameters ρ_1 become negative with $\rho_{g1} < \rho_{l1}$, meaning that the tendency for clustering of like molecules is slightly higher for the gel phase than for the liquid-crystalline phase. The system in which the PA component has the shorter chain, i.e. DMPA:DPPE, has ρ_1 values a factor of five smaller than for the DPPA:DMPE system. For the latter system the formation of mixed pairs is therefore even more likely and also more pronounced for the gel phase.

Pseudobinary systems at pH 4

When the pH is reduced to 4, the charge of pure PAs is reduced to approximately −0.5 elementary charges (Eibl and Blume 1979). Actually, we must consider a composition-dependent apparent pK in the mixtures of PA with PE, because the apparent pK depends on the surface charge density (Träuble et al. 1976; see discussion in Garidel et al. 1997a). Partial protonation of PA has the effect that the non-ideality parameters ρ_1 become more negative at pH 4 than under neutral pH conditions. An exception is found for the system DPPA:DMPE, which still has negative ρ_1 values, however, in contrast with the other systems with negative ρ_1 values we observe: ρ_1(pH 7) < ρ_1(pH 4). The phase diagrams of the systems with the same chain length on both lipids have, again, a similar shape. With the exception of the DPPA:DMPE system, it is found that the phase diagrams DPPA:DPPE, DMPA:DMPE, and DMPA:DPPE at pH 4 with negative ρ_1 and $\rho_{g1} < \rho_{l1}$ have an upper azeotropic point.

The fact that at pH 4 mixed pair formation is favored can be interpreted as a consequence of reduced electrostatic repulsion between the molecules and the increased ability to form a hydrogen-bond network, because of the partial protonation of the PA headgroup.

To illustrate the effect of partial protonation on the miscibility of a PA:PE system, we performed a Monte Carlo simulation of the lateral lipid distribution (Kawasaki 1972; Jan et al. 1984) for the system DPPA:DPPE at pH 7 and pH 4 (Fig. 13). The temperature was set to 70°C (liquid-crystalline phase), with the mole fraction $x_{DPPA} = 0.55$, and the non-ideality parameters were taken from the simulation of the phase diagrams. At pH 7 ρ_1 is positive (+195 cal/mol), indicating clustering of like molecules in the liquid-crystalline phase, however because of the small ρ_1 value the tendency is not pronounced (Fig. 13). At pH 4, at which the non-ideality parameter has changed sign with $\rho_1 = -650$ cal/mol, the arrangement of

the lipids is no longer statistical and mixed pair formation is preferred (Fig. 13).

Pseudobinary systems at pH 12

The thermograms of the PA:PE systems at pH 12 (Figs. 5 and 6) are all very broad compared to those at pH 4 and 7. This is in agreement with the results obtained for the PA:PC systems at pH 12 (Garidel et al. 1997a).

For evaluation of the DSC experiments at pH 12 we have to consider that during the heating scan hydrolysis of the lipids might occur, which would contribute to enthalpic effects. TLC tests of the samples revealed that after the second scan hydrolysis, i.e. formation of lysolipids, occurred, a process which becomes particularly important after the third run when the sample had been at elevated temperatures for a substantial amount of time. We therefore evaluated the heat-capacity curves from the first scan only.

The phase diagrams of the four PA:PE systems all have an upper azeotropic point. However, the phase diagrams of the mixtures DMPA:DMPE and DPPA:DPPE, in which both components have the same chain length, cannot be reliably simulated, as indicated by the dotted lines in Fig. 11. This is different for the other two systems. For the DPPA:DMPE system even a miscibility gap in the liquid-crystalline phase is found. The non-ideality parameters ρ_{l1} are positive with $\rho_{l1} > \rho_{g1}$ indicating preferred demixing in the liquid-crystalline phase. The Gibbs free energy of mixing $\Delta G_{mix} = \Delta G^{ideal} + \Delta G^{E}$, calculated using the non-ideality parameters determined from the phase diagram for the system DPPA:DMPE at 48°C (liquid-crystalline phase), even suggests a fluid–fluid miscibility gap between $x_{DPPA} = 0.5$ and 0.85 (arrows in Fig. 14). Complete miscibility would require that $(\delta^2 \Delta G_{mix}/\delta x^2)_{P,T} > 0$ over the whole composition range. As can be seen in Fig. 14, this is not the case and, therefore, the fluid mixture separates into different phases with compositions indicated by the arrows determined by a common tangent touching the curve. Numerous published diagrams (Huang and Feigenson, 1993) show a symmetric ΔG_{mix} versus x plot. In contrast, the plot represented here is non-symmetric because of our approach of using a two parameter model for the mixing behavior in each phase.

We have calculated the lateral molecular distribution for the DPPA:DMPE system at pH 12 for a mole fraction of $x_{DPPA} = 0.5$ and 0.85 to the left and right of the borders of the miscibility gap. Again we used a Monte Carlo technique (Kawasaki 1972; Jan et al. 1984) using the non-ideality parameters from our simulations of the whole phase diagram (Fig. 12). At pH 12, a mole fraction of $x_{DPPA} = 0.5$ and a temperature of 48°C (fluid phase) the system separates into two different phases with lateral

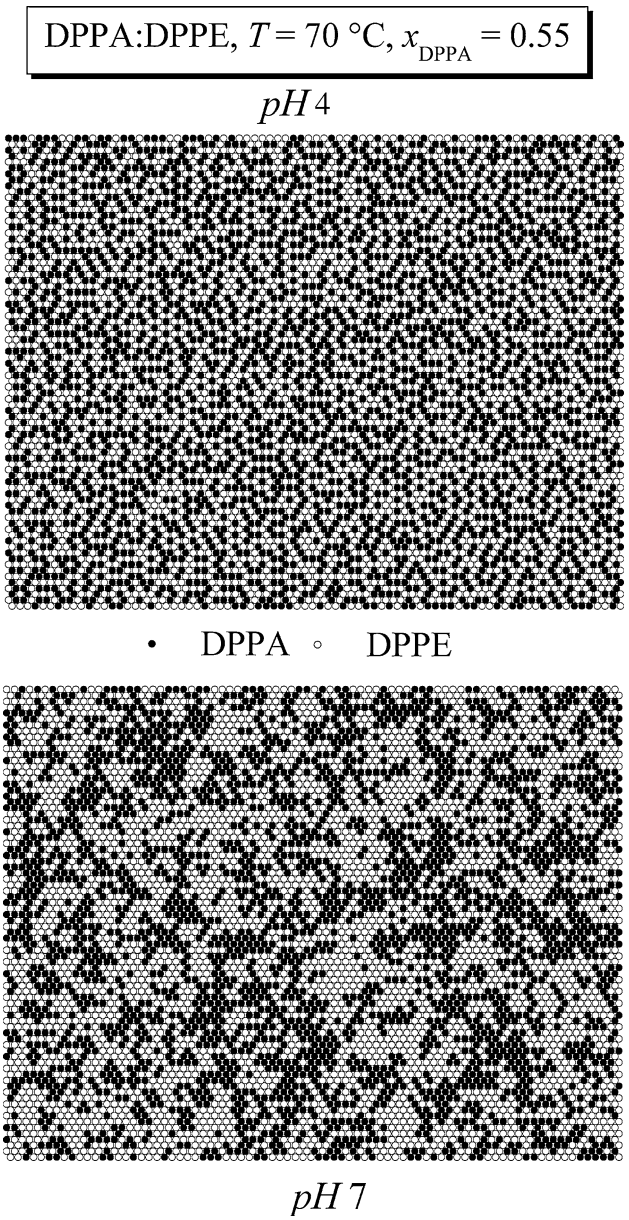

Fig. 13 Lipid lateral distributions in the liquid-crystalline phase (70°C) obtained from Monte Carlo simulations for the system DPPA:DPPE at pH 4 and pH 7. For simulation of the mixture with $x_{DPPA} = 0.55$ the non-ideality parameters used were $\rho_l = -650$ cal/mol (pH 4) and $\rho_l = +190$ cal/mol (pH 7)

distribution of molecules (Fig. 15). As a result of the highly positive non-ideality parameter values, like molecules tend to cluster into domains. At $x_{DPPA} = 0.85$ domains of DMPE molecules in a DPPA matrix are formed.

These results show that the formation of microdomains in the bilayer can occur via changes in headgroup interactions induced by changes in headgroup charge. In contrast with expectations that an increase in charge would favor better mixing of the components because of

electrostatic repulsion, the opposite effect is observed, i.e. a demixing of the components with a clustering of doubly charged PA molecules. This is quite remarkable and emphasizes the results from simulations that the gain in electrostatic energy by separation of charges is small in highly charged systems, because of the close proximity of the charged headgroups.

The clustering of like molecules at pH 12 can also be driven by loss of the ability of PAs to form a hydrogen-bonding network and the fact that in the gel phase PAs are tilted. However, PEs maintain the possibility of forming a hydrogen-bonding network between themselves. These effects arising from the headgroup interactions of the different phospholipids are modulated by the differences in acyl chain length between the components. For systems with different chain lengths (e.g. the system DPPA:DMPE), larger nonideality parameters are usually obtained.

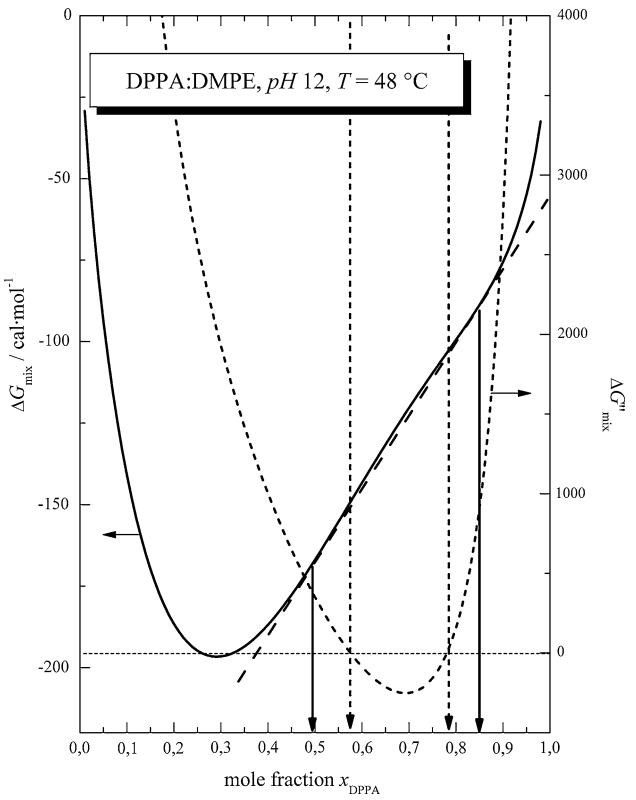

Fig. 14 Calculation of ΔG_{mix} as a function of x_{DPPA} for DPPA:DMPE mixtures at pH 12 using the non-ideality parameters shown in Fig. 12. The boundaries of the region of instability as determined from the 2nd derivative of ΔG_{mix} ($\Delta G''_{mix}$ = short dashed line) are indicated by the *short dashed arrows*. The boundaries of the miscibility gap are shown as *arrows with full lines* as determined from the common tangent method (*dashed line*)

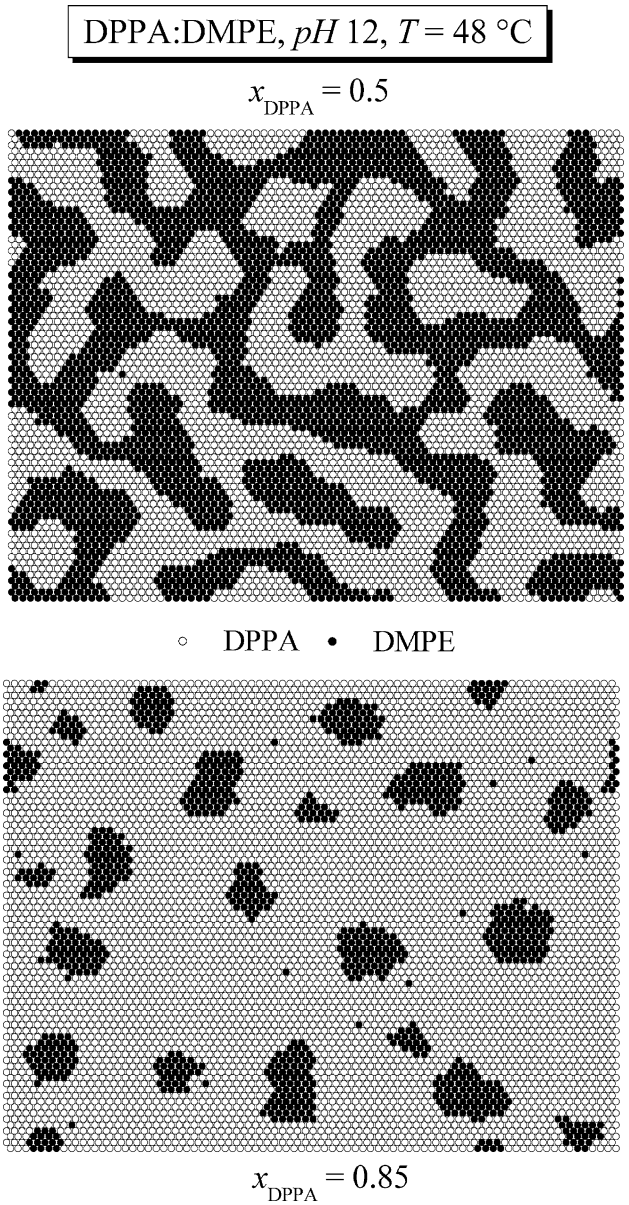

Fig. 15 Lipid lateral distributions in the liquid-crystalline phase (48°C) obtained from Monte Carlo simulations for the system DPPA:DMPE at pH 12. For the simulation for mixtures with $x_{DPPA} = 0.5$ the non-ideality parameter used was $\rho_1 = +1{,}100$ cal/mol and for $x_{DPPA} = 0.85$: $\rho_1 = +782$ cal/mol

Comparison with other mixtures composed of a zwitterionic lipid with a negatively charged lipid and variation of the degree of protonation

Analysis of the mixing behavior of pseudo-binary mixtures composed of a negatively charged lipid (one negative elementary charge) and a zwitterionic phospholipid leads, for most of the systems studied, to the result that mixed pair formation is favored at pH 7. This complex formation by different lipids is much more pronounced in the gel state than in the liquid-crystalline state, because the values for ρ_{g1} are

Table 2 The non-ideality parameters of the PA:PE systems obtained by simulation of the whole phase diagram (Figs. 5, 6, 7, 8, 9, 10, 11, and 12)

System	ρ/cal mol^{-1}															
	pH 4						pH 7						pH 12					
	ρ_{g1}	ρ_{l1}	ρ_{g2}	ρ_{l2}	$\Delta\rho_1$	$\Delta\rho_2$	ρ_{g1}	ρ_{l1}	ρ_{g2}	ρ_{l2}	$\Delta\rho_1$	$\Delta\rho_2$	ρ_{g1}	ρ_{l1}	ρ_{g2}	ρ_{l2}	$\Delta\rho_1$	$\Delta\rho_2$
DMPA:DMPE	−120	+27	+123	−7	+148	−130	+140	+340	−70	−101	+200	−31	+151	+612	+5	+77	+461	+72
DPPA:DPPE	−831	−552	+919	+974	+279	+55	+8	+186	−1	−88	+178	−87	−1,436	−1,110	+1,607	+1,698	+326	+91
DMPA:DPPE	−2,607	−2,517	+703	+486	+90	−217	−1,417	−1,331	+103	−82	+86	−185	−194	+256	+276	+12	+450	−264
DPPA:DMPE	−141	−77	+149	+134	+64	−15	−304	−281	+315	+363	+23	+48	+619	+1,100	+394	+454	+481	+60

ρ_{l1} are both negative and $\rho_{g1} < \rho_{l1}$. The trend with negative non-ideality parameters and $\rho_{g1} < \rho_{l1}$ (DMPA:DPPE and DPPA:DMPE) reported here has also been found for the four PA:PC systems at pH 7 (Garidel et al. 1997a). Replacing the negative lipid component PA by PG, another negatively charged phospholipid (Garidel et al. 1997b), leads to the same result for the non-ideality parameters ρ_1, namely $\rho_{g1} < \rho_{l1}$ and $\rho_1 < 0$ (with an exception for the system DPPE:DMPG, because here $\rho_1 < 0$ but $\rho_{l1} < \rho_{g1}$).

At pH 4, replacement of PE in PA:PE mixtures with a lipid which does not have the ability to form a hydrogen-bonding network at pH 4, e.g. PCs, shows that the non-ideality parameters ρ_1 become less negative or even positive compared with PA:PE systems. Reduction of the electrostatic effects are similar for the PA:PE and PA:PC systems, but an opposite trend for the values of the non-ideality parameters is found for ρ_1 when the pH is changed from 7 to 4. For all the PA:PC systems ρ_1(pH 7) < ρ_1(pH 4) whereas for the PA:PE systems (with the exception for the DPPA:DMPE system) it was found that: ρ_1(pH 7) > ρ_1(pH 4). These results are a good indication that electrostatic effects are compensated by other effects, e.g. formation of a hydrogen-bonding network and hydration effects (Garidel and Blume 2000). Positive or less negative non-ideality parameters ρ_1 with decreasing pH have also been found for the PE:PG systems (Garidel and Blume 2000).

Summary and conclusions

We have analyzed the mixing behavior of PA:PE systems as a function of chain length ($n = 14$, 16) and degree of ionization of the acidic component. The heat-capacity curves were simulated using a previously used model based on regular solution theory, and the phase diagrams were simulated by use of a regular solution model with non-ideal and non-symmetric mixing.

The non-ideality parameters of the systems with the same chain length on both lipid components have positive ρ_1 values at pH 7 for both phases, which indicates clustering of like molecules. In systems with different hydrocarbon chain lengths the two lipids prefer to adopt mixed pair formation, as can be deduced from the non-ideality parameters at pH 7. With the exception of the system DPPA:DMPE, the phase diagram for the systems contain an upper azeotropic point at pH 4 and pH 7. Protonation of the acidic component has the effect that mixed pair formation is favored at pH 4.

Upper azeotropic points or immiscibility in the liquid-crystalline phase at pH 12 is found for the systems DMPA:DMPE, DMPA:DPPE, and DPPA:DMPE. A horizontal liquidus curve is obtained for the last system; this is indicative of a miscibility gap in this region. This shows

that, despite the fact that electrostatic repulsion between the doubly charged headgroups is increased, formation of microdomains occurs in the bilayers of doubly charged PA molecules. This supports results from Monte Carlo simulations with inclusion of electrostatic effects, which indicate that the gain in electrostatic energy by separation of charges is small in highly charged systems, because of the close proximity of the charged headgroups. This gain in energy by charge separation can easily be overcome by other attractive interactions between the headgroups, for example hydrogen bonds.

Our results show that the mixing properties of lipids depend in a subtle way on different properties, namely van der Waals interactions between the chains, electrostatic interactions between the headgroups, and interactions via hydrogen bonds between the headgroups. Whereas the van der Waals interactions between the chains depend, for a given system, on the nature of the fatty acyl chains, the interactions of the headgroups can be modified by changing the pH or salt concentration. In biological systems, the miscibility of lipids can therefore be regulated very quickly by local changes of pH or salt concentration, because of the high mobility of the lipids in the plane of the bilayer.

Acknowledgments We thank L. Mennicke for supplying us with the simulation software for the *cp* curves and for intensive and helpful discussions, and O. Haase and M. Weber for their technical help. This work was supported by the Deutsche Forschungsgemeinschaft and the Fonds der Chemischen Industrie.

References

Akoka S, Tellier C, Poignant S (1986) Molecular order dynamics, and ionization state of phosphatidylethanolamine bilayers as studied by ^{15}N-NMR. Biochemistry 25:6972–6977

Almeida PFF (2009) Thermodynamics of lipid interactions in complex bilayers. Biochim Biophys Acta 1788:72–85

Aloia RC, Curtain CC, Gordon LM (eds) (1988) Advances in membrane fluidity. Lipid domains and their relationship to membrane function, vol 2. Alan. R. Liss, Inc, New York

Benga G, Holmes RP (1984) Interactions between components in biological membranes and their implications for membrane function. Prog Biophys Mol Biol 43:195–257

Blume A (1988) Applications of calorimetry to lipid model membranes. In: Hidalgo C (ed) Physical properties of biological membranes and their functional implications. Plenum Publishing Corporation, New York, pp 71–121

Blume A (1991) Biological calorimetry: membranes. Thermochim Acta 193:299–347

Blume A, Eibl HJ (1979) The influence of charge on bilayer membranes. Calorimetric investigations of phosphatidic acid bilayers. Biochim Biophys Acta 558:13–21

Blume A, Eibl H (1981) A calorimetric study of the thermotropic behavior of 1, 2-dipentadecylmethylidene phospholipids. Biochim Biophys Acta 640:609–618

Blume A, Tuchtenhagen J (1992) Thermodynamics of ion binding to phospholipid bilayers. Titration calorimetry of the heat of dissociation of DMPA. Biochemistry 31:4636–4642

Boggs JM (1987) Lipid intermolecular hydrogen bonding: influence on structural organization and membrane function. Biochim Biophys Acta 906:353–404

Brumbaugh EE, Huang C (1992) Parameter estimation in binary mixtures of phospholipids. Methods Enzymol 210:521–539

Cai TX, Liu PS, Yang FQ, Yang FY (2010) The research advances in the field of lipidomics. Prog Biochem. Biophys. 37:121–128

Cevc G (1990) Membrane electrostatics. Biochim Biophys Acta 1031:311–382

Coskun U, Simons K (2010) Membrane rafting: from apical sorting to phase segregation. FEBS-Lett 584:1685–1693

Cronan JE Jr, Vagelos. RR (1972) Metabolism and function of the membrane phospholipids of *Escherichia coli*. Biochim Biophys Acta 265:25–60

Cronan JE, Gelman EP (1975) Physical properties of membrane lipids: biological relevance and regulation. Bacteriol Rev 39:232–256

Eibl H, Blume A (1979) The influence of charged on phosphatidic acid bilayer membranes. Biochim Biophys Acta 553:476–488

Feigenson GW (2009) Phase diagrams and lipid domains in multicomponent lipid bilayer mixtures. Biochim Biophys Acta 1788:47–52

Gally HU, Pluschke G, Overath P, Seelig J (1980) Structure of *Escherichia coli* membranes. Fatty acyl chain order parameter of inner and outer membranes and derived liposomes. Biochemistry 19:1638–1643

Garidel P (1993) Physikalisch-chemische Untersuchungen zum thermotropen Verhalten von Phospholipiden. Anwendungen der DSD-, DSC-, ^{2}H-NMR- und FT-IR-Methoden. Diploma thesis, University of Kaiserslautern, Germany

Garidel P, Blume A (1998) Miscibility of phospholipids with identical headgroups and acyl chain lengths differing by two methylene units: effects of headgroup structure and headgroup charge. Biochim Biophys Acta 1371:83–95

Garidel P, Blume A (2000) The mixing behavior of pseudobinary phosphatidylethanolamine-phosphatidylglycerol mixtures as a function of *pH* and acyl chain length. Eur Biophys J 28:629–638

Garidel P, Johann C, Blume A (1997a) Nonideal mixing and phase separation in phosphatidylcholine-phosphatidic acid mixtures as a function of acyl chain length and *pH*. Biophys J 72:2196–2210

Garidel P, Johann C, Mennicke L, Blume A (1997b) The mixing behavior of pseudobinary phosphatidylcholine-phosphatidylglycerol mixtures as a function of *pH* and chain length. Eur Biophys J 26:447–459

Garidel P, Johann C, Blume A (2000) Thermodynamics of lipid organization and domain formation in phospholipid bilayers. J. Liposome Res 10(2–3):131–158

Garidel P, Johann C, Blume A (2005) The calculation of heat-capacity curves and phase diagrams based on regular solution theory. J Therm Anal Calorim 82:447–455

Goñi FM, Alonso A, Bagatolli LA, Brown RE, Marsh D, Prieto M, Thewalt JL (2008) Phase diagrams of lipid mixtures relevant to the study of membrane rafts. Biochim Biophys Acta 1781:665–684

Hildebrandt HJ (1929) Solubility (XII). Regular solutions. J Am Chem Soc 51:66–80

Huang J, Feigenson GW (1993) Monte Carlo simulation of lipid mixtures: finding phase separation. Biophys J 65:1788–1794

Jähnig F, Harlos K, Vogel H, Eibl H (1979) Electrostatic interactions at charged lipid membranes. Electrostatically induced tilt. Biochemistry 18:1459–1468

Jan H, Lookman T, Pink DA (1984) On computer simulation methods used to study models of two-component lipid bilayers. Biochemistry 23:3227–3231

Johann C, Garidel P, Mennicke L, Blume A (1996) New approaches for the simulation of heat-capacity curves and phase diagrams of pseudobinary phospholipid mixtures. Biophys J 71:3215–3228

Kawasaki K (1972) Kinetics of Ising models. In: Domb C, Green MS (eds) Phase transitions and critical phenomena. Academic Press, London, pp 443–501

Lee AG (1975a) Functional properties of biological membranes: a physical-chemical approach. Prog Biophys Mol Biol 29:3–56

Lee AG (1975b) Fluorescence studies of chlorophyll a incorporated into lipid mixtures, and the interpretation of "phase" diagrams. Biochim Biophys Acta 413:11–23

Lee AG (1977a) Lipid phase transitions and phase diagrams. I. Lipid phase transitions. Biochim Biophys Acta 472:237–281

Lee AG (1977b) Lipid phase transitions and phase diagrams. II. Mixtures involving lipids. Biochim Biophys Acta 472:285–344

Lee AG (1978) Calculation of phase diagrams for non-ideal mixtures of lipids, and a possible random distribution of lipids in lipid mixtures in the liquid crystalline phase. Biochim Biophys Acta 507:433–444

Lingwood D, Simons K (2010) Lipid rafts as a membrane-organizing principle. Science 327:46–50

Mennicke L (1995) Die Simulation der Wärmekapazitätskurven und die Berechnung der Phasendiagramme von pseudobinären Lipid-Lipid-Wasser Systemen am Beispiel von gemischtkettigen Phospholipiden mit verzweigten Acylketten. PhD thesis, University of Kaiserslautern, Germany

Schimshick EJ, McConnell HM (1973) Lateral phase separation in phospholipid membranes. Biochemistry 12:2351–2360

Shevchenko A, Simons K (2010) Lipidomics: coming to grips with lipid diversity. Nat Rev Mol Cell Biol 11:593–598

Standish MM, Pethica BA (1968) Surface pressure and surface potential study of a synthetic phospholipid at the air/water interface. Trans Faraday Soc 64:1113–1122

Steck TL (1974) The organization of proteins in the human red blood cell membrane. A review. J Cell Biol 62:1–19

Tatulian SA (1992) Ionization and ion binding. In: Cevc G (ed) Phospholipid Handbook. Chap. 14, 511–552

Tenchov B (1985) Nonuniform lipid distribution in membranes. Prog Surf Sci 20:273–340

Träuble H, Eibl HJ (1974) Electrostatic effects on lipid phase transitions: membrane structure and ionic environment. Proc Natl Acad Sci USA 71:214–219

Träuble H, Teubner M, Woolley P, Eibl H (1976) Electrostatic interactions at charged lipid membranes. 1. Effects of *pH* and univalent cations on membrane structure. Biophys Chem 4:319–342

VanGolde LMG, Tomasi V, vanDeenen. LLM (1967) Determination of molecular species of lecithin from erythrocytes and plasma. Chem Phys Lipids 1:282–293

Verkleij AJ, De Kruyff B, Ververgaert PH, Tocanne JF, van Deenen LLM (1974) The influence of *pH*, Ca^{2+} and protein on the thermotropic behaviour of the negatively charged phospholipid, phosphatidylglycerol. Biochim Biophys Acta 39:432–437

Watts A, Poile TW (1986) Direct determination by ^{2}H-NMR of the ionization state of phospholipids and of a local anaesthetic at the membrane surface. Biochim Biophys Acta 861:368–372

Wu SH, McConnell HM (1975) Phase separations in phospholipid membranes. Biochemistry 14:847–854

Ziegler W, Blume A (1995) Acyl chain conformational ordering of individual components in liquid-crystalline bilayers of mixtures of phosphatidylcholines and phosphatidic acids. A comparative FTIR and ^{2}H NMR study. Spectrochim Acta Part A 51:1763–1778